

Fourier computational ghost imaging using spectral sparsity and conjugation priors

Liheng Bian, Jinli Suo, Xuemei Hu, Feng Chen, and Qionghai Dai*

Department of Automation, Tsinghua University, Beijing 100084, China

**Corresponding author: qhdai@tsinghua.edu.cn*

Compiled December 3, 2024

Computational ghost imaging (CGI) retrieves a target scene from numerous random illumination patterns and corresponding single pixel measurements. Theoretically, these random patterns sample random combinations of the Fourier coefficients of the scene's spatial spectrum in an indiscriminative way, and neglect their intrinsic nonuniform importance. Utilizing the sparsity and conjugation priors of natural images' spatial spectra, this letter proposes a new pattern illuminating strategy termed Fourier computational ghost imaging (FCGI), for highly efficient single pixel imaging. Specifically, FCGI sequentially uses two sinusoidal patterns to sample each Fourier coefficient, instead of their random combinations, in the statistically most informative spectrum band. Benefiting from the new illumination patterns and importance sampling strategy, our approach is able to reduce the requisite number of projected patterns by two orders of magnitude, compared to conventional CGI. © 2024 Optical Society of America

OCIS codes: (110.1758) Computational imaging; (120.4820) Optical systems; (110.2970) Image detection systems.

Ghost imaging (GI) originates from quantum optics [1, 2], and later extends to classical light field [3, 4]. It is a novel technique being able to retrieve a spatial resolved scene, from reference beams and corresponding correlated single pixel measurements. Later, Shapiro proposes computational ghost imaging (CGI) [5] using programmable illumination patterns to bypass recording the reference patterns. Specifically, CGI uses a spatial light modulator (SLM) to modulate the illumination to form random patterns, and sequentially projects them onto the scene. A single pixel detector is placed at the end of the light path, to detect all the photons emitted from the scene. As reviewed by Erkmen and Shapiro [6], the extension from conventional GI to CGI largely simplifies the physical implementation, and broadens the applications of ghost imaging systems.

Given both the illumination patterns and single pixel measurements, a reconstruction algorithm is applied to recover the target scene. Existing reconstruction algorithms for CGI can be classified into two categories: (i) linear correlation methods, e.g., traditional GI (TGI) [7], differential GI (DGI) [8] and normalized GI (NGI) [9]; (ii) compressive sensing methods [10, 11]. Comparatively, the former is of easier implementation and higher running efficiency, but requires much more measurements. Therefore, it is time consuming and memory demanding [12, 13] for acquisition. Especially, orders of magnitude times more measurements are needed in real applications, to compensate the system noise and influences from other external factors. As a reference, Sun et al. [14] use around 10^6 measurements (around 20 times of the image pixels) to reconstruct each 256×192 -pixel image owning sufficient quality for subsequent 3D imaging. For the compressive sensing methods, certain priors of the target image are introduced, thus less measurements are needed to produce satisfying results. However, the re-

construction turns into an ill-posed task and the computation complexity increases largely. This makes the compressive sensing methods less competitive [11].

Most recently, Zhang et al. [15] propose not to project random patterns onto the scene. Instead, they design sinusoidal patterns for projection. Each four $\frac{\pi}{2}$ -phase-shifted sinusoidal patterns owning the same single spatial frequency yield the target image's Fourier coefficient at the specific frequency. By sequentially projecting these sinusoidal pattern groups owning different frequencies, the spatial spectrum of the target image can be obtained. Then inverse Fourier transform is applied to reconstruct the scene. Though the method is robust to noise and could produce high quality reconstruction, the requisite number of measurements is still large (2 times of the image pixels in theory).

In this letter, we propose a new pattern illuminating strategy termed Fourier computational ghost imaging (FCGI). FCGI also projects sinusoidal patterns as [15], but differentiates in two aspects: (i) utilizing the sparsity prior of natural images' spectra, FCGI performs importance sampling in the Fourier domain according to the target scene's spectrum distribution, i.e., FCGI doesn't sample all the Fourier coefficients exhaustively; (ii) according to the conjugation property of each centrosymmetric coefficient pair of natural images' spectra, two sinusoidal $\frac{\pi}{2}$ -phase-shifted patterns owning the same spatial frequency are projected onto the scene, instead of four as [15]. Benefitting from these two strategies, FCGI can save most of projections than [15]. In the following, we begin to introduce the proposed FCGI in detail.

Determine the acquisition band. Statistics [16] tell that the spatial spectrum of a natural scene exhibits strong sparsity. Here we first study the statistical distribution of natural scenes' spectra, and accordingly determine the priority of coefficient sampling for

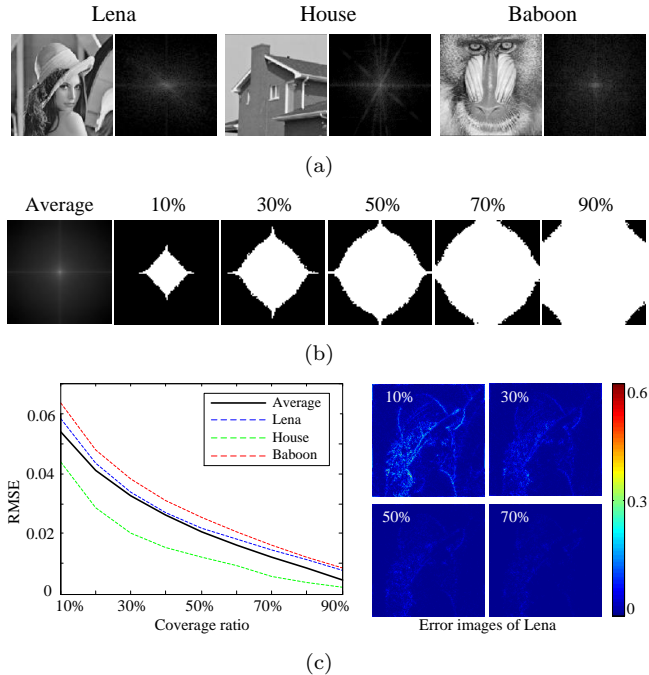


Fig. 1. **Statistical study of natural images' spatial spectra.** (a) Exemplar natural images and corresponding spatial spectra. (b) Average spectrum, and different acquisition bands under different coverage ratios. (c) The relationship between reconstruction error and coverage ratio.

the proposed FCGI. We transform all the 44 images in the USC-SIPI common miscellaneous database [17] to Fourier space, and calculate the average magnitude map of the spectra, as the first image in Fig. 1(b) shows. It is clear that large magnitudes mainly assemble in the low-frequency band. Several exemplar images' spectra shown in Fig. 1(a) also validate this property. Then we threshold the average spectrum to determine the acquisition bands under different coverage ratios (the ratio between the acquisition band and the whole spectrum). The results are shown in Fig. 1(b), where white areas stand for acquisition spectrum bands.

Based on the thresholding results, users can determine the acquisition band by setting coverage ratio according to specific applications, to balance the number of projected patterns and reconstruction error. To further study the relationship between coverage ratio and reconstruction error, we successively sample the spectrum of each image in the dataset under different coverage ratios, transform them back to spatial space, and calculate the reconstruction errors in terms of root-mean-square error (RMSE). The average performance at different coverage ratios is plotted as the black solid curve in Fig. 1(c), and the performance of several exemplar images are plotted with dashed lines, which indicate that different images are of slight diversity, but generally still follow the same trend. Besides, the reconstruction residues of “Lena” at different coverage ratios are displayed on the right side as a reference.

Sample the coefficients. After the acquisition band determined, we begin to design patterns to sample the coefficients of these frequencies. First, we analyze the information encoded by the single pixel measurement, in the view of spatial frequency. According to the Fourier theorem, a two-dimensional image \mathbf{I} can be represented as $\mathbf{I} = \sum_i c_i \mathbf{B}_i$, where \mathbf{B}_i is the i th normalized Fourier basis with the same size as \mathbf{I} , and c_i is its corresponding frequency coefficient. Similarly, by applying Fourier transform to the projected pattern \mathbf{P} , we can get $\mathbf{P} = \sum_j \hat{c}_j \mathbf{B}_j$. The correlated measurement s collected by the single-pixel detector can be represented as

$$\begin{aligned}
 s &= \left| \sum_m \sum_n \mathbf{I}(m, n) \mathbf{P}(m, n) \right| & (1) \\
 &= \left| \sum_m \sum_n \left[\sum_i c_i \mathbf{B}_i(m, n) \right] \left[\sum_j \hat{c}_j \mathbf{B}_j(m, n) \right] \right| \\
 &= \left| \sum_i \sum_j c_i \hat{c}_j \left[\sum_m \sum_n \mathbf{B}_i(m, n) \mathbf{B}_j(m, n) \right] \right|.
 \end{aligned}$$

Here m, n indexes the 2D spatial coordinate. Substituting the orthogonality among Fourier bases

$$f(x) = \begin{cases} \sum_m \sum_n \mathbf{B}_i(m, n) \mathbf{B}_j(m, n) = 0, & i \neq j \\ \sum_m \sum_n \mathbf{B}_i(m, n) \mathbf{B}_j(m, n) = 1, & i = j, \end{cases} \quad (2)$$

into the above equation, we can get

$$s = \left| \sum_j c_j \hat{c}_j \right|. \quad (3)$$

In other words, $\{\hat{c}_j\}$ can be regarded as a spectrum sampling vector. Therefore, we can directly sample a specific frequency's coefficient by setting $\{\hat{c}_j\}$ as a delta function (containing only one non-zero entry).

However, since real facilities can only project real valued patterns, a sinusoidal pattern owns three non-zero coefficients in its spatial spectrum—two conjugate coefficients of a centrosymmetric non-zero frequency pair and one of the zero frequency. The same conjugation property also holds for natural scenes. Let $c_1 = a_0 + jb_0$, $c_2 = a_0 - jb_0$ and $c_3 = d_0$ denote the three non-zero coefficients of the target scene, while $\hat{c}_1 = a_1 + jb_1$, $\hat{c}_2 = a_1 - jb_1$ and $\hat{c}_3 = d_1$ represent corresponding coefficients of a projected sinusoidal pattern \mathbf{P} , we have

$$\begin{aligned}
 s &= |c_1 \hat{c}_1 + c_2 \hat{c}_2 + c_3 \hat{c}_3| & (4) \\
 &= |(a_0 + jb_0)(a_1 + jb_1) + (a_0 - jb_0)(a_1 - jb_1) + d_0 d_1| \\
 &= 2(a_0 a_1 - b_0 b_1) + d_0 d_1.
 \end{aligned}$$

A more explicit demonstration of the derivation is shown in Fig. 2.

So far, sampling a specific Fourier coefficient turns into computing a_0, b_0 , with s, a_1, b_1 and d_1 known. To achieve this, we sequentially project three patterns onto the scene. The first one is a uniform pattern with constant

$$\begin{aligned}
s &= \Sigma \Sigma (\mathbf{I} \odot \mathbf{P}) \\
&= \Sigma \Sigma (\text{Spatial domain}) \\
&= \Sigma \Sigma (\text{Fourier domain}) \\
&= 2(a_0a_1 - b_0b_1) + d_0d_1.
\end{aligned}$$

Fig. 2. Illustration of the encoded scene information by the correlated single pixel measurement when projecting a sinusoidal pattern.

intensity equal to the mean value of pattern \mathbf{P} , and the measurement is exactly d_0d_1 . The other two patterns are sinusoidal patterns respectively with nonzero frequency coefficients as $\{a_1 = \frac{1}{2}, b_1 = 0\}$ and $\{a_1 = 0, b_1 = \frac{1}{2}\}$. Thus we can obtain both a_0 and b_0 by simply subtracting d_0d_1 from the correlated measurements.

Following the above projection method, we can obtain all the important frequencies’ coefficients of the scene, by sequentially projecting sinusoidal patterns owning the same frequencies with the determined acquisition band (note that the uniform pattern needs to be projected only once). Then, the target image can be recovered by applying inverse Fourier transform to the obtained spatial spectrum.

To validate the proposed FCGI, we first conduct a simulation experiment using synthetic data. We set the “Lena” image (128×128 pixels) as the latent scene image, and synthesize the measurements of different patterns following Eq. 1. We set the coverage ratio as 0.1 and 0.3, and correspondingly generate 1638 and 4915 sinusoidal patterns for FCGI reconstruction, respectively. The experiment is conducted using Matlab on an Intel i7 3.6GHz CPU computer, with 16G RAM and 64 bit Windows 7 system. As for comparison, considering its satisfying reconstruction performance, we use DGI [8] to represent the linear correlation methods, and use the augmented Lagrange multiplier method (ALM) [18] to represent the compressive sensing methods. These two methods are applied on the same set of sinusoidal patterns, as well as the same number of random patterns. The results are shown in Fig. 3 and Tab. 1. Note that here we omit the results of “S+DGI”, due to that FCGI and “S+DGI” are intrinsically equivalent. This is because FCGI reconstruction, namely the inverse Fourier transform, is essentially a linear combination of the Fourier bases, which is the same as DGI.

From both the visual and quantitative results, we can clearly see that FCGI largely outperforms conventional

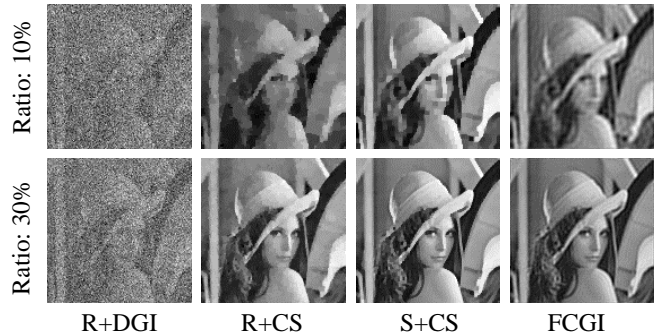


Fig. 3. The simulated reconstruction results of the Lena image by different CGI strategies, with coverage ratio being 10% and 30%, respectively. “R” stands for random patterns, while “S” represents sinusoidal patterns.

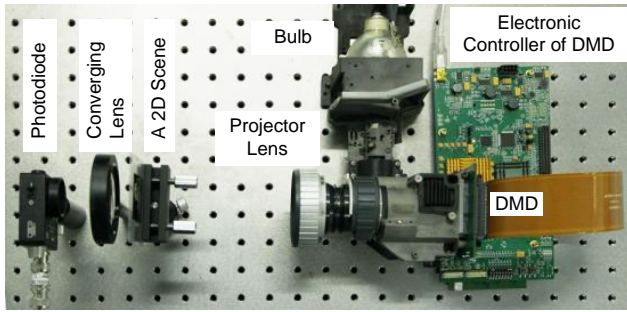
Table 1. Quantitative comparison among different CGI strategies under different coverage ratios.

	Ratio: 10%		Ratio: 30%	
	RMSE	Time	RMSE	Time
R+DGI	0.215	2s	0.191	6s
R+CS	0.115	68min	0.042	92min
S+CS	0.066	67min	0.037	92min
FCGI	0.061	1s	0.044	3s

CGI strategies using random patterns, in terms of both efficiency and reconstruction quality. Note that though CS obtains similar results as FCGI when using sinusoidal patterns, it is much more time consuming and memory demanding. This is because CS models the reconstruction as an ill-posed problem, which needs large memory and long time for computational reconstruction under an optimization framework. Instead, FCGI reconstruction is linear correlation based and doesn’t involve any complex calculations, so it is much faster and memory saving.

To further validate FCGI, we build a prototype exhibited in Fig. 4(a). The system consists mainly two modules: the programmable illumination part and the detection part. The illumination part consists of a projector with its built-in DMD replaced by a Texas Instrument DLP Discovery 4100 Development Kit (.7XGA). We use the 8-bit mode of the DLP to generate patterns, with the frame rate being 30Hz. The 128×128 -pixel patterns are sequentially projected onto a printed transmissive film ($34\text{mm} \times 34\text{mm}$). The correlated rays are collected by a high-speed single-pixel detector (Thorlabs DET100 Silicon photodiode, 340-1100 nm), using a 14-bit acquisition board ART PCI8514. The sampling rate is set as 10000Hz. For each pattern, we average all its corresponding stable measurements for subsequent reconstruction. We set the coverage ratio as 10%, i.e., we project 1638 patterns in all.

The reconstructed results of two different scenes are shown in Fig. 4(b). From the results we can see that



(a)



Target images and spectra

Recovered images and spectra

(b)

Fig. 4. Experiment on real captured data. (a) The prototype. (b) The reconstruction results on two different scenes (128×128 pixels) with coverage ratio being 10%.

10% of the pixel number patterns can yield satisfying results. Compared to [14] where requisite pattern number are 20 times of the pixel number, FCGI could reduce projections by two orders of magnitude.

To better understand the intrinsic advantage of the proposed FCGI over previous studies, we further analyze the information encoding strategies of traditional random patterns and our generative patterns heuristically. Since the spectra of random patterns are also random and thus uniformly distributed, these patterns sample the whole scene’s spectrum uniformly. This prevents conventional CGI from utilizing the importance sampling strategy, and can only simultaneously sample and recover both low-frequency and high-frequency coefficients. This results in its large requisite number of projected patterns. Instead, each sinusoidal pattern only encodes a Fourier coefficient pair at a specific frequency of the scene’s spectrum. Based on this, FCGI could sample only the most informative band according to the spectrum’s distribution, and omit unimportant bands. Thus it is of higher efficiency than conventional random patterns. Besides, utilizing the conjugation property of the real valued image’s spectrum, FCGI could future reduce half the requisite measurements.

In summary, this letter exploits the sparsity and conjugation properties of natural images’ spatial spectra, and proposes a new CGI strategy termed FCGI, which sequentially projects two $\frac{\pi}{2}$ -phase-shifted sinusoidal patterns for each centrosymmetric frequency pair, to con-

duct importance sampling of the scene’s spatial spectrum. FCGI could reduce the requisite number of projected patterns by two orders of magnitude, compared to conventional CGI. Both the simulation and real experiments validate the effectiveness of FCGI.

FCGI can be widely extended. Since the generative representation are additive (Eq. 1), we can adopt multiplexing coding [19] to raise the signal-to-noise-ratio of the final reconstruction. In addition, besides the Fourier transform, there exists many other generative image representation methods (e.g., discrete cosine transform, discrete sine transform). It is interesting to study the pros and cons by applying these transforms to the FCGI framework. What’s more, as the requisite number of patterns is largely reduced, FCGI offers promising potential for real time ghost imaging. These are our future work.

We thank Jihan Li and Jiaqi Ma for their valuable discussions. This work was supported by the National Natural Science Foundation of China (Nos. 61171119, 61120106003, and 61327902).

References

1. T. Pittman, Y. Shih, D. Strekalov, and A. Sergienko, *Phys. Rev. A* **52**, R3429 (1995).
2. D. Strekalov, A. Sergienko, D. Klyshko, and Y. Shih, *Phys. Rev. Lett.* **74**, 3600–3603 (1995).
3. R. S. Bennink, S. J. Bentley, and R. W. Boyd, *Phys. Rev. Lett.* **89**, 113601 (2002).
4. F. Ferri, D. Magatti, A. Gatti, M. Bache, E. Brambilla, and L. Lugiato, *Phys. Rev. Lett.* **94**, 183602 (2005).
5. J. H. Shapiro, *Phys. Rev. A* **78**, 061802 (2008).
6. B. I. Erkmen and J. H. Shapiro, *Adv. Opt. Photon.* **2**, 405–450 (2010).
7. Y. Bromberg, O. Katz, and Y. Silberberg, *Phys. Rev. A* **79**, 053840 (2009).
8. F. Ferri, D. Magatti, L. Lugiato, and A. Gatti, *Phys. Rev. Lett.* **104**, 253603 (2010).
9. B. Sun, S. S. Welsh, M. P. Edgar, J. H. Shapiro, and M. J. Padgett, *Opt. Express* **20**, 16892–16901 (2012).
10. O. Katz, Y. Bromberg, and Y. Silberberg, *Appl. Phys. Lett.* **95**, 131110 (2009).
11. M. Aβmann and M. Bayer, *Sci. Rep.* **3**, 1–5 (2013).
12. B. I. Erkmen and J. H. Shapiro, *Phys. Rev. A* **79**, 023833 (2009).
13. R. Meyers, K. S. Deacon, and Y. Shih, *Phys. Rev. A* **77**, 041801 (2008).
14. B. Sun, M. P. Edgar, R. Bowman, L. E. Vittert, S. Welsh, A. Bowman, and M. Padgett, *Science* **340**, 844–847 (2013).
15. Z. Zhang, X. Ma, and J. Zhong, *Nat. Commun.* **6** (2015).
16. M. W. Marcellin, Springer (2002).
17. Univeisity of Southern California, <http://sipi.usc.edu/database/>, accessed 1/2/15.
18. Z. Lin, M. Chen, and Y. Ma, arXiv preprint arXiv:1009.5055 (2010).
19. Y. Y. Schechner, S. K. Nayar, and P. N. Belhumeur, *IEEE T. Pattern Anal.* **29**, 1339–1354 (2007).

References

1. T. Pittman, Y. Shih, D. Strelakov, and A. Sergienko, "Optical imaging by means of two-photon quantum entanglement," *Phys. Rev. A* **52**, R3429 (1995).
2. D. Strelakov, A. Sergienko, D. Klyshko, and Y. Shih, "Observation of two-photon 'ghost' interference and diffraction," *Phys. Rev. Lett.* **74**, 3600–3603 (1995).
3. R. S. Bennink, S. J. Bentley, and R. W. Boyd, "'Two-photon' coincidence imaging with a classical source," *Phys. Rev. Lett.* **89**, 113601 (2002).
4. F. Ferri, D. Magatti, A. Gatti, M. Bache, E. Brambilla, and L. Lugiato, "High-resolution ghost image and ghost diffraction experiments with thermal light," *Phys. Rev. Lett.* **94**, 183602 (2005).
5. J. H. Shapiro, "Computational ghost imaging," *Phys. Rev. A* **78**, 061802 (2008).
6. B. I. Erkmen and J. H. Shapiro, "Ghost imaging: from quantum to classical to computational," *Adv. Opt. Photon.* **2**, 405–450 (2010).
7. Y. Bromberg, O. Katz, and Y. Silberberg, "Ghost imaging with a single detector," *Phys. Rev. A* **79**, 053840 (2009).
8. F. Ferri, D. Magatti, L. Lugiato, and A. Gatti, "Differential ghost imaging," *Phys. Rev. Lett.* **104**, 253603 (2010).
9. B. Sun, S. S. Welsh, M. P. Edgar, J. H. Shapiro, and M. J. Padgett, "Normalized ghost imaging," *Opt. Express* **20**, 16892–16901 (2012).
10. O. Katz, Y. Bromberg, and Y. Silberberg, "Compressive ghost imaging," *Appl. Phys. Lett.* **95**, 131110 (2009).
11. M. A β mann and M. Bayer, "Compressive adaptive computational ghost imaging," *Sci. Rep.* **3**, 1–5 (2013).
12. B. I. Erkmen and J. H. Shapiro, "Signal-to-noise ratio of gaussian-state ghost imaging," *Phys. Rev. A* **79**, 023833 (2009).
13. R. Meyers, K. S. Deacon, and Y. Shih, "Ghost-imaging experiment by measuring reflected photons," *Phys. Rev. A* **77**, 041801 (2008).
14. B. Sun, M. P. Edgar, R. Bowman, L. E. Vittert, S. Welsh, A. Bowman, and M. Padgett, "3D computational imaging with single-pixel detectors," *Science* **340**, 844–847 (2013).
15. Z. Zhang, X. Ma, and J. Zhong, "Single-pixel imaging by means of Fourier spectrum acquisition," *Nat. Commun.* **6** (2015).
16. M. W. Marcellin, "JPEG2000: image compression fundamentals, standards, and practice," Springer (2002).
17. Univeisity of Southern California, "SIPI Image Database," <http://sipi.usc.edu/database/>, accessed 1/2/15.
18. Z. Lin, M. Chen, and Y. Ma, "The augmented Lagrange multiplier method for exact recovery of corrupted low-rank matrices," arXiv preprint arXiv:1009.5055 (2010).
19. Y. Y. Schechner, S. K. Nayar, and P. N. Belhumeur, "Multiplexing for optimal lighting," *IEEE T. Pattern Anal.* **29**, 1339–1354 (2007).